eNeuro

Research Article: New Research | Disorders of the Nervous System

Lytic cell death in specific microglial subsets is required for preventing atypical behavior in mice

https://doi.org/10.1523/ENEURO.0342-20.2020

Cite as: eNeuro 2021; 10.1523/ENEURO.0342-20.2020

Received: 9 August 2020
Revised: 15 December 2020
Accepted: 17 December 2020

Manuscript Title Page

1. Manuscript Title

Lytic cell death in specific microglial subsets is required for preventing atypical behavior in mice

2. Abbreviated Title

Microglial lytic cell death prevents atypical behaviors

3. List of authors and affiliations

Hsiu-Chun Chuang[1,4], Eva K. Nichols[1,4], Isabella Rauch[1,2,5], Wei-Cheng Chang[1], Patrick M. Lin[1], Rhea Misra[1], Maiko Kitaoka[1], Russell E. Vance[1,2], Kaoru Saijo[1,3]

1. Division of Immunology and Pathogenesis, Department of Molecular and Cell Biology
2. Howard Hughes Medical Institute
3. Helen Wills Neuroscience Institute
   University of California, Berkeley
   439A LSA, Berkeley, CA 94720-3200, USA
4. These authors equally contributed to this work
5. Present address: Department of Molecular Microbiology and Immunology, Oregon Health & Science University

4. Author contribution

H-C.C. and E.K.N. designed and performed experiments and analyzed data. W-C.C., P.M.L., R.M., and M.K. performed experiments. I.R. and R.E.V. provided critical mouse lines and advice. K.S. conceived and designed the project and wrote the manuscript with input from all authors.

5. Corresponding author

Kaoru Saijo (ksaijo@berkeley.edu)

6. Number of Figures

Main 5
Extended 5

7. Number of Tables

Extended 4

8. Number of Multimedia

2 (Extended Movie)

9. Number of words for Abstract

228 words

10. Number of words for Significance Statement

121 words

11. Number of words for Introduction

678 words

12. Number of words for Discussion

913 words

13. Acknowledgement

We thank the Saijo lab for discussion and E. Robey for critical reading of the manuscript. We also thank H. Aaron and J.Y. Lee for imaging analysis help and A. Sullivan (Obrizus Communications) for editing.

14. Conflict of interest

Authors report no conflict of interest

15. Funding source

E.K.N. was supported by the Chancellor's Fellowship, Elizabeth Roboz Einstein Fellowship, and UC dissertation year fellowship. I.R. is supported by the Austrian Science Fund (the Erwin Schrödinger Fellowship). M.K. is supported by MCB departmental grant 4T32GM07232-40 and NSF GRFP. R.E.V. is an HHMI Investigator and is supported by NIH grants AI075039 and AI063302. K.S. is supported by a NIH grant (R01HD092093), a Searle Scholarship, a Hellman Fellowship, and a Pew Scholarship.

Abstract

Microglial cells are known to contribute to brain development and behaviors, but the mechanisms behind such functions are not fully understood. Here, we show that mice deficient in inflammasome regulators, including caspase-1 (*Casp1*), *Nlrp3*, IL-1 receptor (*Il-1r)*, and gasdermin D (*Gsdmd*), exhibit behavior abnormalities characterized by hyperactivity and low anxiety levels. Furthermore, we found that expression of *Casp1* in CX3CR1^{+} myeloid cells, which includes microglia, is required for preventing these abnormal behaviors. Through tissue clearing and 3D imaging, we discovered that small numbers of *Cx3cr1*-GFP^{+} fetal microglial cells formed clusters and underwent lytic cell death in the primitive thalamus and striatum between embryonic days E12.5 and E14.5. This lytic cell death was diminished in *Casp1*-deficient mice. Further analysis of the microglial clusters showed the presence of Pax6^{+} neural progenitor cells (NPCs); thus, we hypothesized that microglial lytic cell death is important for proper neuronal development. Indeed, increased numbers of neurons were observed in the thalamic subset in adult *Casp1*$^{-/-}$ brains. Finally, injection of drug inhibitors of NLRP3 and CASP1 into wild-type pregnant mice from E12.5 to E14.5, the period when lytic cell death was detected, was sufficient to induce atypical behaviors in offspring. Taken together, our data suggests that the inflammasome cascade in microglia is important for regulating neuronal development and normal behaviors, and that genetic or pharmacological inhibition of this pathway can induce atypical behaviors in mice.

Significance Statement

Microglia support brain development, but the underlying mechanisms are not fully understood. Here, we show that mice deficient for inflammasome cascade protein genes, including *Nlrp3*, *Casp1*, *Il-1r*, and *Gsdmd*, develop behavior abnormalities characterized by hyperactivity and low anxiety. Lytic cell death occurs downstream of inflammasomes and was observed to appear in microglia in spatiotemporal and *Casp1*-dependent manners. Microglial death may be important for the proper differentiation of NPCs, as indicated by increased neuron numbers in specific regions of the brain in *Casp1*-deficient mice. Importantly, injection of NLRP3 and CASP1 inhibitors into pregnant mothers during this lytic death window resulted in offspring with behavior abnormalities. Overall, the death of discrete microglial subsets may be essential for proper NPC development and normal behaviors.

Introduction

Normal brain development is a series of complex events that can be affected by either genetic or environmental factors. Disruptions in these events can result in neurodevelopmental disorders, such as attention-deficit/hyperactivity disorder (ADHD), autism, and intellectual disabilities characterized by atypical behaviors. Interestingly, cell death by apoptosis has been shown to be essential for normal brain development by controlling the number of neurons in the brain and by helping to establish functional circuits (Yoshida et al., 1998; Yamaguchi and Miura, 2015; Fricker et al., 2018); however, it has not yet been reported whether other types of cell death (lytic cell death such as pyroptosis) are also important for regulating these developmental processes.

Microglial cells are resident innate immune cells in the central nervous system that protect the brain from infection and injury; however, recent studies indicate that they are also crucial for brain development and normal functions (Saijo and Glass, 2011; Ransohoff and El Khoury, 2015; Wolf et al., 2017). For example, a patient with a homozygous mutation in the *CSF1R* gene, which plays essential roles in microglial development, lacked microglia and showed severe defects in brain development (Oosterhof et al., 2019). It has also been reported that microglia-mediated synaptic regulation plays crucial roles in the establishment and maintenance of neural circuits (Paolicelli et al., 2011; Hong et al., 2016). However, the molecular mechanisms behind how microglia shape these circuits and affect their corresponding behaviors are not well understood.

Inflammasomes are cytosolic sensors for a variety of pathogenic and noxious stimuli (Rathinam and Fitzgerald, 2016). In the brain, previous reports suggest that inflammasomes are differentially expressed in different cell types. For example, NLR family pyrin domain containing 1 (NLRP1) and AIM2 were detected in neurons, while NLRP2 and NLRP3 were found in astrocytes (Mamik and Power, 2017; Heneka et al., 2018; Voet et al., 2019). Microglia were also observed to express various inflammasomes, particularly NLRP1, NLRP3, and NLRC4 were highly expressed in this cell type (Walsh et al., 2014; Mamik and Power, 2017; Heneka et al., 2018; Voet et al., 2019). Activated inflammasomes serve as platforms that initiate the cleavage of pro-caspase-1 to caspase-1 (CASP1), which then cleaves pro-IL-1β to generate a mature cytokine. CASP1 also cleaves gasdermin D (GSDMD), which is required for subsequent

IL-1β secretion, lytic cell death (pyroptosis), and inflammation (Kayagaki et al., 2015; Shi et al., 2015) (Figure 1-1A).

The importance of the inflammasome pathway in protecting the host from infection and injury is well established (Broz and Dixit, 2016). In addition to being a sentinel, it has also been reported that the inflammasome protein NLRP3 in microglia recognizes amyloid-β peptide and induces an inflammatory response that contributes to the pathogenesis of Alzheimer's disease (Heneka et al., 2013). The idea that NLRP3 plays a role in Alzheimer's disease has been further supported by recent evidence indicating that NLRP3 regulates tau phosphorylation and aggregation (Ising et al., 2019). Thus, inflammasomes can be involved in the onset and progression of neurological disorders; however, their role in early brain development is not understood or expected.

Previous literature has shown that mice deficient for interleukin-1 receptor (*Il-1r*) exhibit hyperactivity and low anxiety levels (Murray et al., 2013). Since mature IL-1β is the product of inflammasome activation, we hypothesized that this pathway might be required for normal brain development and behavior. To test our hypothesis, we ran a panel of behavior assays using mice deficient for factors of the inflammasome cascade and found that they exhibited specific behavior abnormalities. Moreover, during normal development, we observed that lytic cell death occurred in subsets of *Cx3cr1*-GFP^{+} brain parenchymal microglial cells, particularly those located in the primitive thalamus and striatum, but this death was notably absent in mice lacking *Casp1*. Furthermore, administration of inhibitors of NLRP3 and CASP1 to wild-type pregnant female mice at specific gestational days induced behavior abnormalities in their offspring that were similar to those observed in the knockout mice. Overall, our data suggests that the

inflammasome cascade mediated by *Nlrp3*, *Casp1*, *Il-1r*, and *Gsdmd* in microglia is important for normal brain development and for preventing abnormal behaviors in mice.

Materials and Methods

Animals

Both male and female mice (aged 2 to 4 months old) were used in this study. All animals were maintained in specific pathogen-free conditions under a 12-hr light-dark cycle (7 am to 7 pm) and were given a standard chow diet and water *ad libitum*. Wild-type C57BL/6J mice were purchased from The Jackson Laboratory. *Casp1*$^{-/-}$*Casp11*$^{-/-}$ mice were on the C57BL/6J background and were kindly provided by A. Van der Velden and M. Starnbach (van der Velden et al., 2003). *Casp1*$^{-/-}$, *iCasp1*, *Nlrp3*$^{-/-}$, and *Gsdmd*$^{-/-}$ mice on the C57BL/6J background were generously provided by R.E. Vance (Rauch et al., 2017). Tg(*Cx3cr1*-cre)MW126Gsat mice were generated by the Heintz laboratory at The Rockefeller University and were purchased from MMRRC (UC Davis). We backcrossed the Tg(*Cx3cr1*-cre)MW126Gsat mice to C57BL/6J mice more than 10 times before crossing with other strains. *Il-1r*$^{-/-}$ and *Cx3cr1*$^{GFP/GFP}$ mice were on the C57BL6/J background and were purchased from The Jackson Laboratory. To normalize gut microbiota, all animals were cohoused in mixed-genotype groups of 3-5 mice per cage upon weaning. If cohousing was not done, their bedding was mixed regularly to normalize the microenvironment. All experiments were approved by the Animal Care and Use Committee and were performed under the institutional guidelines.

Behavior assays

201 Open field assay

202 For the experiments with *Casp1*$^{-/-}$ mice, both male and female mice were used, as
203 indicated. For the experiments with *Il-1r*$^{-/-}$, *Gsdmd*$^{-/-}$, *Nlrp3*$^{-/-}$ and *iCasp1* (re-expression
204 and their controls) mice, only male mice were used. We also used only male offspring
205 from inhibitor-injected mothers for this assay. Mice were individually placed in the center
206 of a plastic box (22 x 42.5 x 21 cm) for 1 hour and were allowed to freely explore the
207 arena. The data from the first 30 minutes of exploration were used in our analysis
208 (Komada et al., 2008; Jiang et al., 2010; Chung et al., 2011). Animal movement was
209 monitored by computerized photobeam using the MotorMonitor SmartFrame System
210 (Kinder Scientific).
211
212 Elevated plus maze assay
213 We used both male and female *Casp1*$^{-/-}$ mice (as indicated), male *Il-1r*$^{-/-}$, *Gsdmd*$^{-/-}$,
214 *Nlrp3*$^{-/-}$ and *iCasp1* (re-expression and their controls) mice, as well as male offspring
215 from inhibitor-injected mothers for this assay. Mice were individually placed in the center
216 of a platform (5 x 5 cm) of a maze that consisted of two open and two closed arms (30 x
217 5 cm) that were elevated 30 cm from the floor. Mice were allowed to freely explore the
218 maze for 10 min (Lin and Hsueh, 2014; Nakajima et al., 2019; Shieh and Yang, 2019)
219 and the Smart Video Tracking System (Panlab) was used to determine the time spent in
220 the open and closed arms, as well as the center, during the test. The number of entries
221 into each arm was also analyzed.
222
223 Five-choice serial reaction time task (5-CSRTT) assay

Casp1$^{-/-}$ and WT male mice were used for this assay. The procedures used in this task were as previously described with modifications (Sanchez-Roige et al., 2012). A Plexiglas operator chamber (19 x 22 x 24 cm) with five response apertures and a food magazine was automatically controlled by the software (Packwin, Panlab). The procedure consisted of the pre-training, magazine training, and 5-CSRTT training phases. Before the test and then throughout the entire experiment, the mice were food-restricted (1.8-2 g per day). On the first day of food restriction, the mice were introduced to some reward pellets (TestDiet 14 mg sugar pellets) to familiarize them with their taste. During the pre-training phase, mice were habituated to the chamber with five reward pellets in the food magazine and one reward pellet in each of the five apertures being placed for each operant chamber. The magazine light and all five stimulus lights remained illuminated for the duration of the session. The mice were individually placed in the chamber and allowed to freely explore for 10 minutes. The habituation session was repeated until all the pellets were consumed. On the day of magazine training, the mice were placed in the chamber for a 4-min period of free exploration, followed by all five stimulus lights being switched on throughout the remainder of the session. After a random nose-poke response was made in one of the five apertures, the mouse was given 1 pellet in the food magazine. Once the mice earned 20 pellets, they commenced the 5-CSRTT training, which graduates through increasingly challenging stages (stage 1-6) on a schedule of progressively decreasing stimulus duration (SD) and increasing inter-trial intervals (ITI). The percentage of accuracy was calculated as [(number of correct trials/(number of correct and incorrect trials)) x 100]. The number of days taken to achieve the criteria for stage 6 (accuracy > 75%, correct trials > 20) was recorded to

indicate the attention performance. After meeting the criteria of stage 6 for at least two consecutive days, mice were moved forward in the testing schedule in which the variable ITI (5, 8.75, and 12.5 seconds) was randomly presented with an SD of 1.25 s. The percent accuracy was also calculated in this testing.

PI injection and tissue clearing

A total volume of 100 µl of propidium iodide (PI, 1.0 mg/ml) solution was intravenously injected into pregnant female mice at specific gestational dates. After 10-30 min of incubation, the mice were sacrificed. Intact fetal bodies were recovered, fixed, and subjected to the CUBIC tissue clearing method (Susaki et al., 2014).

Light sheet fluorescence microscopy (LSFM) and analysis

We used male embryos that resulted from crossing WT or *Casp1*$^{-/-}$ mice with *Cx3cr1*-GFP mice for this assay. LSFM was performed using the ZEISS Lightsheet Z.1 system and 5X objective set (EC Plan-Neofluar 5x/0.16 detection and LSFM 5x/0.1 illumination lens) at 0.36x zoom. CUBIC R2 solution was used as the refractive index-matched solution. Coronal acquisitions captured the entirety of the embryonic forebrain (about 620 Z slices) with voxel sizes approx. X=2.13 µm, Y=2.13 µm, and Z=6.16 µm. Imaging data was processed and analyzed by Imaris 9.1.0 software (Bitplane).

Immunofluorescence staining

We used male WT and *Casp1*$^{-/-}$ embryos and adult brains for this assay. Intact tissues were fixed in 4% PFA in PBS overnight at 4°C and underwent complete sucrose

gradient up to 30% wt/vol in PBS. Tissues were next embedded in a 1:1 mix of TissueTek O.C.T. compound with 30% sucrose in PBS and sectioned (40 μm sections) with a cryostat. Slides were dried and permeabilized with 0.1% Triton X-100 in PBS. After blocking, sections were incubated with primary antibodies (see Table 1) followed by secondary antibodies.

Drug administration to mice

Pregnant C57BL/6 mice were given three intraperitoneal (i.p.) injections of either VX-765 (50 mg/kg/day, Caspase-1 inhibitor, InvivoGen), MCC950 (50 mg/kg/day, NLRP3-inflammasome inhibitor, InvivoGen), or Saline as vehicle. Drugs were injected once per day starting on E12.5 until E14.5. Behavioral assays were performed on the male offspring when they were 8-weeks old.

RNA extraction and RT-qPCR

Total RNA was isolated using the DirectZol kit (Zymo research). RT reactions were performed using SuperScript III (ThermoFisher) and qPCR was performed using the KAPA SYBR Green Fast qPCR kit by following the manufacturer's protocols. Primers used in this assay were as follows:

Hprt (F 5'-TCAGTCAACGGGGGACATAAA-3', R 5'-GGGGCTGTACTGCTTAACCAG-3'), *Casp1* (F 5'-TGGGACCCTCAAGTTTTGCCC-3', R 5'-GGCAAGACGTGTACGAGTGGTT-3'),

Nlrp3 (F 5'-CTTTGCTGCGATCAACAGGCG-3', R 5'-TCAAGGCTGTCCTCCTGGCATA-3'),

Cd200 (F 5'-TCACTTGCTCTGCGACTGCC-3', R 5'-GGGGTCTTTGACCCGGAGGA-3'),

Celf4 (F 5'-CAAGGAGCGCACAATGCGAC-3', R 5'-ATGAGGGCTGCTTGCTGCTG-3')

Nissl staining and Stereology

Three adult age-matched WT and *Casp1*$^{-/-}$ male mice underwent transcardial perfusion with PBS and 4% PFA in PBS and post-fixation overnight in 4% PFA in PBS. Brains were embedded in O.C.T. compound (Sakura VWR) before serial sectioning at 40 µm in a cryostat. For Nissl staining, sections were stained in Cresyl Violet solution (0.3% wt/vol Cresyl Violet Acetate in water plus 0.3% glacial acetic acid v/v; Sigma C-1791 and 537020) for 45 minutes. Sections were rinsed in ddH_2O and subjected to an ethanol dehydration series (1-minute steps; 70%, 95%, 100% EtOH) before clearing in Xylenes for 3 minutes (Sigma 214736). Sections were mounted in Permount and dried for 24-48 hours before imaging.

The Cavalieri volume estimation method (MicroBrightField) was used to estimate the volume of the thalamus of three adult age-matched WT and *Casp1*$^{-/-}$ mouse brains (from approximately Bregma -1 mm to +4 mm). Nissl-stained sections (40µm) were visualized using the brightfield setting on a BX51 microscope (Olympus) connected to a computer running Stereo Investigator 11.03 software (MicroBrightField). Afterwards, markers were placed (using a grid spacing of 50 µm and a section evaluation interval of 6) over these regions for a total of 11 slices throughout the thalamus. Contours were drawn according to regions defined by the Allen Brain Atlas. Total volumes were then determined using the built-in software estimator. All volume estimations except for one possessed a Gundersen coefficient of error < 0.10.

320

321 **Statistical analysis**

322 Data are shown as averages with error bars indicating S.E.M. Sample sizes were
323 calculated based on the Boston University IACUC spread sheet. Statistical analysis was
324 performed using Prism 7 (GraphPad) software. We used the Student's *t*-test to compare
325 two different groups (Figure 1A-B, 1E-F, 4C, 4E, and Figure 1-1B-F, 1-1I-J, 2-1A-D, 3-
326 1D, 4-1), and we used the one-way ANOVA with *post-hoc* tests (Bartlett's test and
327 Brown-Forsythe test) to compare three different groups (Figure 1C-D, 2B-C, 5B-C, and
328 Figure 1-1G-H, 2-1E-G, 5-1A-B). In addition to one-way ANOVA, Tukey's multiple
329 comparison tests were performed to show the individual *p*-values. The data was
330 provided to the figure legends. The Fisher's exact test was used to analyze contingency
331 tables to determine the probability that the distributions were not due to chance (Figure
332 3E and Figure 3-1A). Table 3 shows the *t*-values, degrees of freedom (df), and *p*-values
333 for the Student's *t*-tests, and Table 4 shows the sum-of-squares (SS), degrees of
334 freedom (DF), the mean squares (MS), F-ratios, and *p*-values for the one-way ANOVA
335 analyses of variation between columns, within columns, and total for the indicated
336 figures. *P*-values < 0.05 were considered to be statistically significant.

337

338 **Results**

339 **Mice deficient for genes regulating the inflammasome cascade exhibit behavior**
340 **abnormalities.**

341 Since a previous report showed that *Il-1r*$^{-/-}$ mice exhibit aberrant behaviors, such
342 as hyperactivity and low anxiety (Murray et al., 2013), we decided to use a panel of

343 behavior assays to assess the global impact of inflammasomes on mouse brain
344 development (Table 1). We first investigated the role of CASP1 in mouse brain because
345 it is a common downstream target of inflammasomes and because multiple
346 inflammasome complexes are expressed in microglia and macrophages (Walsh et al.,
347 2014). We found that male *Casp1*$^{-/-}$ mice showed hyperactivity (Figure 1A) and low
348 anxiety levels (Figure 1B, Figure 1-1B and C), as determined by the open field and
349 elevated plus maze assays (respectively), that were similar to the behavior
350 abnormalities observed in *Il-1r*$^{-/-}$ mice. We also noticed that male *Casp1*$^{-/-}$ mice showed
351 less attention to light stimuli compared to WT mice, as measured by the 5-choice serial
352 reaction time task (Figure 1-1D) (Sanchez-Roige et al., 2012). However, we did not
353 observe other behavioral abnormalities, including decreased sociability, defective
354 learning and memory, or increased restricted repetitive behavior (data not shown).
355 Interestingly, these behavior changes were only observed in male, but not female,
356 *Casp1*$^{-/-}$ mice (Figure 1 A and B (male), Figure 1-1E and F (female)), which is consistent
357 with several reports suggesting that some neurodevelopmental disorders show sex
358 dimorphisms (Rucklidge, 2010).

359 Since both GSDMD and pro-IL-1β are cleaved by CASP1 (Figure 1-1A) as part of
360 the inflammasome pathway, we also used *Gsdmd*- and *Il-1r*-deficient mice (Kayagaki et
361 al., 2015; Shi et al., 2015) in our behavior studies. Our results showed that *Gsdmd*$^{-/-}$
362 mice exhibited hyperactivity (Figure 1C) and low anxiety (Figure 1D, Figure 1-1G and
363 H). Furthermore, consistent with the previous report, we observed behavior
364 abnormalities in *Il-1r*$^{-/-}$ mice, although to a lesser extent (Figure 1C and D, Figure 1-1G
365 and H). Next, we hypothesized that NLRP3 might be the inflammasome protein

responsible for the activation of CASP1 in the fetal brain because NLRP3 detects tissue damage rather than infection (Cassel and Sutterwala, 2010) and because the developing brain in the uterus should be a sterile environment. In addition, NLRP3 could be activated by ATP and ions released from dying/dead cells, given the widespread death of newly differentiated neurons during fetal brain development (Watson, 2012). To test this hypothesis, we ran our behavior assays on *Nlrp3*$^{-/-}$ mice and found that they also exhibited hyperactivity (Figure 1E) and low anxiety (Figure 1F, Figure 1-1I and J). From these results, we concluded that the NLRP3-CASP1-GSDMD/IL-1β pathway is required for establishing normal behavior in mice.

Re-expression of *Casp1* in CX3CR1^{+} cells restores normal behaviors.

The expression of chemokine receptor CX3CR1 is characteristic for myeloid-lineage cells, including microglial cells. In the brain, CX3CR1^{+} cells in the parenchyma are considered microglial cells; however, there are some neutrophils and subsets of macrophages in the meninges and blood vessels that also express CX3CR1. (Mizutani et al., 2012; Wolf et al., 2013). Our gene expression studies showed that *Casp1* and *Nlrp3* mRNAs were highly expressed in CX3CR1^{+} cells, including microglia and macrophages, isolated from fetal brain (Figure 2-1A and B). In contrast, CX3CR1^{-} cells displayed high expression levels of *Cd200* and *Celf4* mRNAs, which are associated with neural cells (Figure 2-1C and D) (Haimon et al., 2018). Because the *Casp1*$^{-/-}$ mice used in our initial studies were conventional knockout mice in which *Casp1* was deleted from all cell types, *Casp1*$^{-/-}$ mice expressing a Cre-inducible *Casp1* allele (*Rosa26-LoxP-STOP-LoxP-Casp1-IRES-GFP*, *iCasp1* mice) (Rauch et al., 2017) were crossed to BAC

389 transgenic mice expressing Cre under the control of the *Cx3cr1* promoter, a commonly
390 used Cre-driver enriched in microglia (Wolf et al., 2013), so that *Casp1* would be re-
391 expressed in CX3CR1^{+} cells. The resulting *Casp1*$^{-/-}$; *iCasp1*; *Cx3cr1*-Cre (Experimental)
392 mice and their *Casp1*$^{-/-}$; *iCasp1* littermate controls (Control, equivalent to *Casp1*$^{-/-}$;
393 Figure 2A) as well as wild-type (WT) mice were then used in our previously described
394 behavior assays (Table 2) to verify that re-expression of *Casp1* in immune cells is
395 necessary for preventing behavior abnormalities and ensuring normal brain
396 development. Remarkably, re-expression of *Casp1* in CX3CR1^{+} cells (Figure 2-1E)
397 resulted in animals without hyperactivity (Figure 2B) or low anxiety levels (Figure 2C,
398 Figure 2-1F and G); thus, we concluded that *Casp1* expression in CX3CR1^{+} myeloid
399 cells, including microglial cells, plays an essential role in establishing normal behaviors.
400
401 **Lytic cell death occurs in a spatiotemporal manner in the mouse fetal brain.**
402 Lytic cell death, downstream of the inflammasome pathway, has been described
403 in macrophages and dendritic cells as well as in aged microglia in the context of
404 Alzheimer's disease (Heneka et al., 2013). However, it is not known whether microglia
405 undergo lytic cell death during fetal brain development. Because mice deficient for
406 *Gsdmd*, a factor that is essential for the induction of lytic cell death (Shi et al., 2015),
407 exhibited behavior abnormalities similar to those observed in *Casp1*-deficient mice
408 (Figure 1A-D), we hypothesized that fetal microglia might undergo lytic cell death. To
409 investigate whether microglial cell death occurs during early brain development,
410 propidium iodide (PI; a DNA dye) was used to visualize dying microglia. PI is able to
411 stain these cells because during lytic cell death, plasma membrane integrity is lost,

allowing the dye into the cells (Fink and Cookson, 2005; Zhang et al., 2018). For this assay, PI was injected into pregnant WT females that had been crossed with *Cx3cr1*$^{GFP/GFP}$ male mice at specific days during fetal brain development. The genotype of the resulting offspring was *Cx3cr1*$^{GFP/+}$, with microglia that were labeled with GFP (Jung et al., 2000). While it is known that *Cx3cr1* is expressed in non-microglial cells outside the brain, *Cx3cr1*-GFP^{+} cells in the brain parenchyma are considered microglia (Mizutani et al., 2012). Following PI injection, embryos were recovered, the tissue was cleared using the CUBIC method (Susaki et al., 2014), and the brains were imaged via light sheet fluorescence microscopy (LSFM; Figure 3A). Interestingly, our imaging revealed discrete clusters of GFP^{+}PI^{+} cells in both the lateral ganglionic eminence (LGE), which matures into a major part of the striatum, and the intermediate thalamus (iTh) starting at E12.5 (Figure 3B, Figure 3-1A). These clusters were also noted in both the LGE and iTh at E14.5 (Figure 3C and E, Figure 3-1B, Movie 1), coincident with active neurogenesis and neuronal cell death (Watson, 2012). Clusters were comprised of 20-200 microglial cells, with averages of 107 and 85 cells/cluster in the LGE and iTh, respectively, at E14.5 (Figure 3-1B) and fewer cells at E12.5 (data not shown). To determine whether the cells in the clusters experienced lytic cell death, we measured the diameters of GFP^{+} and GFP^{+}PI^{+} cells and found that GFP^{+}PI^{+} cells had significantly larger diameters, suggesting that these cells had lost membrane integrity and were swollen (Figure 3-1C and D).

Since CASP1 activation is required for lytic cell death (Figure 1-1A), we next tested whether the observed cell death was impaired in *Casp1*$^{-/-}$ mice. Using *Cx3cr1*$^{GFP/GFP}$ mice crossed with *Casp1*$^{-/-}$ mice, we found that the formation of GFP^{+}PI^{+}

cell clusters in the LGE and iTh was significantly reduced in *Casp1*$^{-/-}$; *Cx3cr1*-GFP offspring at E14.5 (Figure 3D and E, Movie 2). Conversely, in *Casp1*$^{-/-}$; *iCasp1*; *Cx3cr1*-Cre (Experimental) mice, which express GFP following Cre-mediated recombination (Rauch et al., 2017) (Figure 2A), we observed GFP^{+} cells that were also positive for PI signal (Figure 3-1E). Overall, these results suggest that microglia in the LGE and iTh undergo lytic cell death during fetal brain development at E12.5-E14.5 in a *Casp1*-dependent manner.

The TRN region in *Casp1*$^{-/-}$ brains has increased numbers of neurons.

In mice, neural progenitor cells (NPCs) start to differentiate at E12.5, coincident with the microglial lytic cell death that we observed in the fetal brain. Therefore, we hypothesized that defective microglial cell death might influence NPCs in the developing brain. To determine whether there were NPCs in the GFP^{+}PI^{+} clusters, we performed our LSFM analysis on *Cx3cr1*$^{GFP/+}$ mice, with the addition of anti-Pax6 antibodies to stain Pax6^{+} NPCs in the brain. Our imaging showed that the GFP^{+}PI^{+} clusters were indeed associated with NPCs in the fetal brain (Figure 4A). Based on this result, we hypothesized that defective lytic cell death of microglia might contribute to alterations in brain structures resulting from improper development of NPCs and neurons derived from the LGE and iTh. To test our hypothesis, we measured the volumes of major parts of the cerebrum as well as descendants of the LGE (striatum) and iTh (thalamus) and found that there were no differences between adult WT and *Casp1*$^{-/-}$ mice (Figure 4-1) in these areas.

457 Because we did not observe gross structural anomalies in the thalamus, or
458 striatum, we next tested whether we could observe finer compositional changes. Since
459 previous reports have suggested that IL-1β plays important roles in NPC death,
460 proliferation, and differentiation (Crampton et al., 2012; Guadagno et al., 2015), and
461 because the timing of these events are prior to circuit establishment, we hypothesized
462 that defective microglial lytic cell death may change the numbers of cells located within
463 structures descending from the LGE and iTh. Therefore, we serially sectioned entire
464 cerebrums of adult WT and *Casp1*$^{-/-}$ mice and then immunostained them with anti-NeuN
465 antibody to identify neurons. While we did not find obvious cellular changes in regions
466 descending from the LGE, we found increased numbers of neurons in the thalamic
467 reticular nucleus (TRN; parvalbumin^{+} cells) a region developed from the iTh, in *Casp1*$^{-/-}$
468 mice (Figure 4B and C). These results suggest that appropriate microglial lytic cell
469 death may be important for regulating proper neuronal numbers in certain brain
470 compartments.
471
472 **Increased microglial numbers are not observed in the TRN of adult *Casp1*$^{-/-}$ mice.**
473 Since the death of fetal microglia in *Casp1*$^{-/-}$ mice was impaired, and microgliosis
474 (increased numbers of microglia) is often associated with pathological conditions in the
475 brain (Lull and Block, 2010; Bruck et al., 2016), we hypothesized that the number of
476 microglia in the TRN might be increased, resulting in disrupted neuronal homeostasis.
477 To test this hypothesis, we measured the number of microglia using anti-Iba1 antibody
478 staining in the TRN. Our results showed that despite the lack of lytic cell death in

Casp1$^{-/-}$ mice, microglial numbers in the TRN were not increased (Figure 4D and E), suggesting that the behavior abnormalities observed in these mice are not due to microgliosis in the brain.

Injecting inflammasome pathway inhibitors into dams results in behavioral abnormalities in offspring.

Since we observed that lytic cell death occurred on specific days during fetal brain development and microglial death might be necessary for the proper differentiation of NPCs, we hypothesized that inhibition of the NLRP3-CASP1-GSDMD/IL-1β pathway during this developmental window might be sufficient to induce behavior abnormalities similar to those observed in *Casp1*$^{-/-}$ mice. To test this hypothesis, WT pregnant mothers were injected with specific drug inhibitors of CASP1 and NLRP3 (VX-765 and MCC950, respectively) (Coll et al., 2015) at E12.5, E13.5, and E14.5, times when we observed lytic cell death in WT fetal brains, and then behavior assays were performed on the offspring to determine their activity and anxiety levels (Figure 5A). Our results showed that male offspring from MCC950-injected mice (and, to a lesser extent, VX-765-injected mice) showed hyperactivity (Figure 5B) and low anxiety levels (Figure 5C, Figure 5-1A and B). These results suggest that pharmacological disruption of the NLRP3/CASP1 pathway, especially NLRP3 inhibition (MCC950), during development may be sufficient to induce the behavior abnormalities observed in our knockout mice. Our working model is that the NLRP3-CASP1-GSDMD/IL-1β cascade in microglia is essential for normal brain development, and that genetic or pharmacological disruption of this pathway leads to aberrant behavior in mice (Figure 5D). We also propose that

disruption of this pathway may impact the development of NPCs, thus resulting in increased numbers of neurons in the TRN, a region descendant from the iTh, which may cause atypical behaviors in mice.

Discussion

In this study, we have shown that the NLRP3-CASP1-GSDMD/IL-1β cascade in microglia is required for normal brain development and prevents behavior abnormalities such as hyperactivity and low anxiety levels (Figure 1). *Casp1* and *Nlrp3* are predominantly expressed in CX3CR1^{+} myeloid-lineage cells in the fetal brain, and our data showed that the re-expression of *Casp1* in these cells in *Casp1*-deficient mice restored normal behaviors (Figure 2). These results indicate the importance of myeloid cells, particularly microglia, in early brain development to ensure normal behaviors in mice.

The current study shows that microglial lytic cell death occurs in a spatiotemporal manner, with small subsets of microglia in the iTh and LGE undergoing death from E12.5 to E14.5. The timing of microglial death during development is essential since NPCs start to differentiate at E12.5 in the mouse brain. It is also possible that active cell death occurs in NPCs and newly differentiated neurons in and around this timeframe. Thus, dead or dying NPCs and neurons could release ATP and K^{+} that could trigger the NLRP3 cascade in microglia, resulting in the cleavage of pro-IL1β to its mature form (He et al., 2016). It has been reported that microglial IL-1β is required for NPC differentiation and death (Crampton et al., 2012; Guadagno et al., 2015), so we attempted to measure the amount of secreted IL-1β in the ventricles of the fetal brain by

ELISA assay. IL-1β levels were found to be below the level of detection (data not shown), but we assume that this was because only a small number of cells underwent lytic cell death (Figure 3-1B). However, despite the undetectable levels of IL-1β in the fetal brain, we and another group found that *Il-1r*$^{-/-}$ mice exhibit behavior abnormalities (Murray et al., 2013 and this manuscript), suggesting that IL-1β does indeed play a role in ensuring normal behavior development in mice.

Since we observed that Pax6^{+} NPCs were a part of PI^{+}*Cx3cr1*-GFP^{+} clusters (Figure 4A), and neural circuits are important for behavior, we reasoned that we should look for alterations in neurons as a consequence of defective lytic cell death in *Casp1*$^{-/-}$ microglia to explain the atypical behaviors observed in our inflammasome pathway knockout mice. We did not observe global changes in brain structures in the striatum and thalamus descendent from the LGE and iTh (Figure 4-1) in adult *Casp1*$^{-/-}$ brains; however, we did confirm increased numbers of neurons in the TRN (Figure 4B and C), a region descending from the microglial lytic cell death zone observed in developing *Casp1*$^{-/-}$ mice. Interestingly, a recent report suggested that the TRN regulates a circuit required for attention and hyperactivity (Wells et al., 2016), behavior abnormalities that were observed in *Casp1*$^{-/-}$ mice (Figure 1A and B, Figure 1-1B-D). As discussed above, this increase in neurons could have been due to a lack of IL-1β production in microglia that resulted in impaired death and/or differentiation of NPCs. Alternatively, we could speculate that microglial engulfment of NPCs might be decreased since we observed that mRNA expression of *Mrc2*, a gene known to be involved in phagocytosis, was decreased in *Casp1*$^{-/-}$ microglia isolated from adult mice (data not shown). However, since we did not observe the deregulation of other genes regulating phagocytosis in

548 *Casp1*$^{-/-}$ microglia isolated from adult mice, it is difficult to conclude whether this process
549 is actually impaired. Thus, it would be of interest to study the phagocytic activity of
550 microglia in mice deficient for genes regulating the NLRP3-CASP1-GSDMD/IL-1β
551 cascade. Furthermore, additional studies are required to determine whether the
552 functions of neurons in the TRN are also altered to explain the behavior abnormalities
553 observed in mice.

554 Since increased numbers of microglia (microgliosis) are often associated with
555 pathological conditions, such as neurodegenerative diseases (Lull and Block, 2010;
556 Bruck et al., 2016), we expected that defective microglial death would lead to increased
557 microglial cell numbers in regions descendent from the iTh and LGE, thus altering
558 neural functions. However, we did not observe increased numbers of microglia in the
559 TRN. Lytic cell death of microglia was found to occur primarily in the LGE and iTh
560 regions of the brain. Recent reports suggest that microglia might be transcriptionally
561 heterogenous, indicating that specific microglial subsets may exist in different areas in
562 the brain (Li et al., 2019; Masuda et al., 2019). If this is the case, the lytic cell death that
563 we observed may be occurring only in specific subsets of microglia located in these
564 regions. Based on these results, it is clear that specific microglial lytic cell death has an
565 impact on normal brain development; however, the precise mechanism of this regulation
566 and the interplay between specific microglia and NPCs/neurons in the developing brain
567 warrant further study.

568 Impressively, injection of NLRP3 and CASP1 inhibitors into pregnant wild-type
569 mice during the time frame of microglial death resulted in behavior abnormalities in their
570 offspring that recapitulated those observed in the NLRP3 pathway knockout mice.

These results suggest that disruption of this pathway during this key developmental window is sufficient to significantly alter normal brain development and behavior. Since the NLRP3-CASP1-GSDMD/IL-1β cascade in microglia is crucial for normal brain development, and either genetic or pharmacological disruption of this pathway can lead to atypical behavior in mice (Figure 5D), we propose that pro-inflammatory cytokines, such as IL-1β, may play essential roles in regulating the differentiation and proliferation of NPCs (Figure 5-1C). Therefore, the numbers and functions of neurons descending from the LGE and iTh may be altered in mice with defects in the NLRP3-CASP1-GSDMD/IL-1β cascade, which could contribute to their behavioral phenotypes.

References

Broz P, Dixit VM (2016) Inflammasomes: mechanism of assembly, regulation and signalling. Nat Rev Immunol 16:407-420.

Bruck D, Wenning GK, Stefanova N, Fellner L (2016) Glia and alpha-synuclein in neurodegeneration: A complex interaction. Neurobiol Dis 85:262-274.

Cassel SL, Sutterwala FS (2010) Sterile inflammatory responses mediated by the NLRP3 inflammasome. Eur J Immunol 40:607-611.

Chung WC, Huang TN, Hsueh YP (2011) Targeted deletion of CASK-interacting nucleosome assembly protein causes higher locomotor and exploratory activities. Neurosignals 19:128-141.

Coll RC et al. (2015) A small-molecule inhibitor of the NLRP3 inflammasome for the treatment of inflammatory diseases. Nat Med 21:248-255.

Crampton SJ, Collins LM, Toulouse A, Nolan YM, O'Keeffe GW (2012) Exposure of foetal neural progenitor cells to IL-1beta impairs their proliferation and alters their differentiation - a role for maternal inflammation? J Neurochem 120:964-973.

Fink SL, Cookson BT (2005) Apoptosis, pyroptosis, and necrosis: mechanistic description of dead and dying eukaryotic cells. Infect Immun 73:1907-1916.

Fricker M, Tolkovsky AM, Borutaite V, Coleman M, Brown GC (2018) Neuronal Cell Death. Physiol Rev 98:813-880.

Guadagno J, Swan P, Shaikh R, Cregan SP (2015) Microglia-derived IL-1beta triggers p53-mediated cell cycle arrest and apoptosis in neural precursor cells. Cell Death Dis 6:e1779.

Haimon Z, Volaski A, Orthgiess J, Boura-Halfon S, Varol D, Shemer A, Yona S, Zuckerman B, David E, Chappell-Maor L, Bechmann I, Gericke M, Ulitsky I, Jung S (2018) Re-evaluating microglia expression profiles using RiboTag and cell isolation strategies. Nat Immunol 19:636-644.

He Y, Hara H, Nunez G (2016) Mechanism and Regulation of NLRP3 Inflammasome Activation. Trends Biochem Sci 41:1012-1021.

Heneka MT, McManus RM, Latz E (2018) Inflammasome signalling in brain function and neurodegenerative disease. Nat Rev Neurosci 19:610-621.

Heneka MT, Kummer MP, Stutz A, Delekate A, Schwartz S, Vieira-Saecker A, Griep A, Axt D, Remus A, Tzeng TC, Gelpi E, Halle A, Korte M, Latz E, Golenbock DT (2013) NLRP3 is activated in Alzheimer's disease and contributes to pathology in APP/PS1 mice. Nature 493:674-678.

Hong S, Dissing-Olesen L, Stevens B (2016) New insights on the role of microglia in synaptic pruning in health and disease. Curr Opin Neurobiol 36:128-134.

Ising C et al. (2019) NLRP3 inflammasome activation drives tau pathology. Nature 575:669-673.

Jiang YH, Pan Y, Zhu L, Landa L, Yoo J, Spencer C, Lorenzo I, Brilliant M, Noebels J, Beaudet AL (2010) Altered ultrasonic vocalization and impaired learning and memory in Angelman syndrome mouse model with a large maternal deletion from Ube3a to Gabrb3. PLoS One 5:e12278.

Jung S, Aliberti J, Graemmel P, Sunshine MJ, Kreutzberg GW, Sher A, Littman DR (2000) Analysis of fractalkine receptor CX(3)CR1 function by targeted deletion

and green fluorescent protein reporter gene insertion. Mol Cell Biol 20:4106-4114.

Kayagaki N et al. (2015) Caspase-11 cleaves gasdermin D for non-canonical inflammasome signalling. Nature 526:666-671.

Komada M, Takao K, Miyakawa T (2008) Elevated plus maze for mice. J Vis Exp.

Li Q, Cheng Z, Zhou L, Darmanis S, Neff NF, Okamoto J, Gulati G, Bennett ML, Sun LO, Clarke LE, Marschallinger J, Yu G, Quake SR, Wyss-Coray T, Barres BA (2019) Developmental Heterogeneity of Microglia and Brain Myeloid Cells Revealed by Deep Single-Cell RNA Sequencing. Neuron 101:207-223 e210.

Lin CW, Hsueh YP (2014) Sarm1, a neuronal inflammatory regulator, controls social interaction, associative memory and cognitive flexibility in mice. Brain Behav Immun 37:142-151.

Lull ME, Block ML (2010) Microglial activation and chronic neurodegeneration. Neurotherapeutics 7:354-365.

Mamik MK, Power C (2017) Inflammasomes in neurological diseases: emerging pathogenic and therapeutic concepts. Brain 140:2273-2285.

Masuda T, Sankowski R, Staszewski O, Bottcher C, Amann L, Sagar, Scheiwe C, Nessler S, Kunz P, van Loo G, Coenen VA, Reinacher PC, Michel A, Sure U, Gold R, Grun D, Priller J, Stadelmann C, Prinz M (2019) Spatial and temporal heterogeneity of mouse and human microglia at single-cell resolution. Nature 566:388-392.

Mizutani M, Pino PA, Saederup N, Charo IF, Ransohoff RM, Cardona AE (2012) The fractalkine receptor but not CCR2 is present on microglia from embryonic development throughout adulthood. J Immunol 188:29-36.

Murray CL, Obiang P, Bannerman D, Cunningham C (2013) Endogenous IL-1 in cognitive function and anxiety: a study in IL-1RI-/- mice. PLoS One 8:e78385.

Nakajima R, Takao K, Hattori S, Shoji H, Komiyama NH, Grant SGN, Miyakawa T (2019) Comprehensive behavioral analysis of heterozygous Syngap1 knockout mice. Neuropsychopharmacol Rep 39:223-237.

Oosterhof N, Chang IJ, Karimiani EG, Kuil LE, Jensen DM, Daza R, Young E, Astle L, van der Linde HC, Shivaram GM, Demmers J, Latimer CS, Keene CD, Loter E, Maroofian R, van Ham TJ, Hevner RF, Bennett JT (2019) Homozygous Mutations in CSF1R Cause a Pediatric-Onset Leukoencephalopathy and Can Result in Congenital Absence of Microglia. Am J Hum Genet 104:936-947.

Paolicelli RC, Bolasco G, Pagani F, Maggi L, Scianni M, Panzanelli P, Giustetto M, Ferreira TA, Guiducci E, Dumas L, Ragozzino D, Gross CT (2011) Synaptic pruning by microglia is necessary for normal brain development. Science 333:1456-1458.

Ransohoff RM, El Khoury J (2015) Microglia in Health and Disease. Cold Spring Harb Perspect Biol 8:a020560.

Rathinam VA, Fitzgerald KA (2016) Inflammasome Complexes: Emerging Mechanisms and Effector Functions. Cell 165:792-800.

Rauch I, Deets KA, Ji DX, von Moltke J, Tenthorey JL, Lee AY, Philip NH, Ayres JS, Brodsky IE, Gronert K, Vance RE (2017) NAIP-NLRC4 Inflammasomes Coordinate Intestinal Epithelial Cell Expulsion with Eicosanoid and IL-18 Release via Activation of Caspase-1 and -8. Immunity 46:649-659.

673 Rucklidge JJ (2010) Gender differences in attention-deficit/hyperactivity disorder.
674 Psychiatr Clin North Am 33:357-373.
675 Saijo K, Glass CK (2011) Microglial cell origin and phenotypes in health and disease.
676 Nat Rev Immunol 11:775-787.
677 Sanchez-Roige S, Pena-Oliver Y, Stephens DN (2012) Measuring impulsivity in mice:
678 the five-choice serial reaction time task. Psychopharmacology (Berl) 219:253-
679 270.
680 Shi J, Zhao Y, Wang K, Shi X, Wang Y, Huang H, Zhuang Y, Cai T, Wang F, Shao F
681 (2015) Cleavage of GSDMD by inflammatory caspases determines pyroptotic cell
682 death. Nature 526:660-665.
683 Shieh KR, Yang SC (2019) Exploratory and agile behaviors with central dopaminergic
684 activities in open field tests in Formosan wood mice (Apodemus semotus). J Exp
685 Biol 222.
686 Susaki EA, Tainaka K, Perrin D, Kishino F, Tawara T, Watanabe TM, Yokoyama C,
687 Onoe H, Eguchi M, Yamaguchi S, Abe T, Kiyonari H, Shimizu Y, Miyawaki A,
688 Yokota H, Ueda HR (2014) Whole-brain imaging with single-cell resolution using
689 chemical cocktails and computational analysis. Cell 157:726-739.
690 van der Velden AW, Velasquez M, Starnbach MN (2003) Salmonella rapidly kill
691 dendritic cells via a caspase-1-dependent mechanism. J Immunol 171:6742-
692 6749.
693 Voet S, Srinivasan S, Lamkanfi M, van Loo G (2019) Inflammasomes in
694 neuroinflammatory and neurodegenerative diseases. EMBO Mol Med 11.
695 Walsh JG, Muruve DA, Power C (2014) Inflammasomes in the CNS. Nat Rev Neurosci
696 15:84-97.
697 Watson CP, G.; Puelles, L. (2012) The mouse nervous system.
698 Wells MF, Wimmer RD, Schmitt LI, Feng G, Halassa MM (2016) Thalamic reticular
699 impairment underlies attention deficit in Ptchd1(Y/-) mice. Nature 532:58-63.
700 Wolf SA, Boddeke HW, Kettenmann H (2017) Microglia in Physiology and Disease.
701 Annu Rev Physiol 79:619-643.
702 Wolf Y, Yona S, Kim KW, Jung S (2013) Microglia, seen from the CX3CR1 angle. Front
703 Cell Neurosci 7:26.
704 Yamaguchi Y, Miura M (2015) Programmed cell death in neurodevelopment. Dev Cell
705 32:478-490.
706 Yoshida H, Kong YY, Yoshida R, Elia AJ, Hakem A, Hakem R, Penninger JM, Mak TW
707 (1998) Apaf1 is required for mitochondrial pathways of apoptosis and brain
708 development. Cell 94:739-750.
709 Zhang Y, Chen X, Gueydan C, Han J (2018) Plasma membrane changes during
710 programmed cell deaths. Cell Res 28:9-21.
711

712 **Figure Legends**

713 **Figure 1. Mice deficient for inflammasome pathway genes exhibit behavior**
714 **abnormalities.** This figure is supported by Extended Figure 1-1. **A.** General activity of
715 male WT (black circles, N=11, from 5 litters) and *Casp1*$^{-/-}$ (red triangles, N=12, from 5
716 litters) mice was determined by open field assay and is shown as total distance moved
717 (centimeters, cm). p=0.0049, df=21, t=3.142. **B.** Anxiety levels of male WT and *Casp1*$^{-/-}$
718 mice were determined using the elevated plus maze assay and are shown as time
719 spent in open arms (sec). p=0.0029, df=21, t=3.371. **C and D.** General movement (**C**)
720 and anxiety levels (**D**) of male WT (black circles, N=13, from 4 litters), *Il-1r*$^{-/-}$ (blue
721 squares, N=10, from 3 litters), and *Gsdmd*$^{-/-}$ (green triangles, N=11, from 4 litters) mice
722 were determined as in A and B, respectively. (C) p=0.0159, DF=33, F=4.748. Tukey's
723 multiple comparison test: WT vs *Il-1r*$^{-/-}$ p=0.0147, WT vs *Gsdmd*$^{-/-}$ p=0.1270, *Il-1r*$^{-/-}$ vs
724 *Gsdmd*$^{-/-}$ p=0.5866. (D) p=0.0050, DF=33, F=6.306. Tukey's multiple comparison test:
725 WT vs *Il-1r*$^{-/-}$ p=0.1809, WT vs *Gsdmd*$^{-/-}$ p=0.0036, *Il-1r*$^{-/-}$ vs *Gsdmd*$^{-/-}$ p=0.2727. **E and**
726 **F.** General movement (**E**) and anxiety (**F**) of male WT (black circles, N=10, from 3
727 litters) and *Nlrp3*$^{-/-}$ mice (orange diamonds, N=9, from 2 litters) were determined as in A
728 and B, respectively. (E) p=0.0220, df=17, t=2.520. (F) p=0.0130, df=17, t=2.776. Data
729 shown are individual mice and error bars indicate S.E.M. Asterisk (*) shows p<0.05, and
730 (**) shows p<0.01.

731

732 **Figure 2. *Casp1* re-expression in CX3CR1^{+} cells restores normal behavior.** This
733 figure is supported by Extended Figure 2-1. **A.** Experimental design is shown. Three
734 mouse lines (*Casp1*$^{-/-}$, *iCasp1*, and *Cx3cr1*-Cre) were crossed to generate *Casp1*$^{-/-}$;

735 *iCasp1*; *Cx3cr1*-Cre positive mice (Experimental) and *Casp1*$^{-/-}$; *iCasp1*; Cre negative
736 littermates (Control). Mice expressing Cre had induced expression of *Casp1* in
737 CX3CR1^{+} cells, but not in CX3CR1^{-} cells. **B.** General movement of male WT (black
738 circles, N=7, from 3 litters), littermate Control (blue triangles, N=6, from 4 litters), and
739 Experimental (red squares, N=12, from 8 litters) mice was determined by open field
740 assay and is shown as total distance moved (centimeters, cm). p=0.0581, DF=24,
741 F=3.247. Tukey's multiple comparison test: WT vs Control p=0.0997, WT vs
742 Experimental p=0.5502, Control vs Experimental p=0.3072. **C.** Anxiety levels of male
743 WT (black circles, N=7, from 3 litters), Control (blue triangles, N=10, from 6 litters), and
744 Experimental (red squares, N=12, from 8 litters) mice were determined by elevated plus
745 maze assay and are shown as time spent in open arms (sec). p<0.0001, DF=28,
746 F=15.97. Tukey's multiple comparison test: WT vs Control p<0.0001, WT vs
747 Experimental p=0.0760, Control vs Experimental p=0.0023. Data indicates individual
748 animals and error bars are shown as S.E.M. Asterisk (****) indicates p<0.0001 and n.s.
749 indicates not significant.
750
751 **Figure 3. Lytic cell death occurs in a spatiotemporal manner in the fetal brain.**
752 This figure is supported by Extended Figure 3-1 and Movie 1 and 2. **A.** Experimental
753 scheme is shown. Propidium Iodide (PI) was injected into pregnant female mice at
754 specific gestational stages. Ten to thirty minutes after PI injection, total fetal bodies
755 were recovered, cleared, and imaged by LSFM. **B.** Representative sagittal and coronal
756 LSFM images of the LGE and primitive intermediate thalamus (iTh) of a WT E12.5 fetal
757 brain (male, N=6, from 2 litters) are shown. Arrows indicate the cluster. Green: GFP,

Purple: PI. Scale bars indicate 500 μm. **C.** Representative images of a WT E14.5 fetal brain (male, N=6, from 3 litters) are shown. Arrows indicate the cluster. Green: GFP, Purple: PI. Scale bars indicate 500 μm. **D.** Representative coronal LSFM images of a *Casp1*$^{-/-}$ brain (male, N=5, from 3 litters) at E14.5 are shown. Scale bars indicate 500 μm. **E.** Numbers of mice that exhibited clusters in the LGE and iTh at E14.5 are shown. Asterisk (*) indicates $p<0.05$ and (**) shows $p<0.01$.

Figure 4. Numbers of neurons but not microglia are increased in the TRN in adult *Casp1*$^{-/-}$ mice. This figure is supported by Extended Figure 4-1. **A**. Enlarged image of the GFP^{+}PI^{+} cluster shown in Figure 3. Mice were injected with PI as shown in Figure 3A and fetal brain slices were stained with anti-Pax6 antibody. Images of *Cx3cr1*-GFP (top left), PI (top right), anti-Pax6 (bottom left), and merged signals are shown. Scale bar indicates 50 μm. **B**. Representative images of anti-NeuN staining signals from male *Casp1*$^{-/-}$ (N=3, right, from 2 litters) and sex/age-matched WT (N=3, left, from 2 litters) adult brains are shown. TRN regions are outlined in yellow. Scale bar indicates 200 μm. **C.** Average anti-NeuN signals from *Casp1*$^{-/-}$ (red triangles) and WT (black circles) mice are shown as cell number/mm^2. Dots indicate individual animals and are the average cell numbers from a total of 6 serial sections stained as shown in B. $p=0.0209$, df=4, $t=3.694$. Error bars indicate S.E.M. and asterisk (*) indicates $p<0.05$. **D.** Representative images of anti-Iba1 antibody staining in the TRNs (regions outlined in yellow) of male WT (N=3, left, from 2 litters) and *Casp1*$^{-/-}$ (N=3, right, 2 litters) mice are shown. Scale bar indicates 200 μm. **E.** Average number of Iba1^{+} cells in *Casp1*$^{-/-}$ (red triangles) and WT (black circles) mice are shown as mean cell number/mm^2. Dots indicate individual

781 animals and are the average of cell numbers from a total of 6 serial sections stained as
782 shown in D. *p*=0.7533, df=4, *t*=0.336. Error bars indicate S.E.M. and n.s. indicates not
783 significant.
784
785 **Figure 5. Fetal exposure to inflammasome inhibitors leads to aberrant behaviors.**
786 This figure is supported by Extended Figure 5-1. **A.** Experimental scheme is shown.
787 Pregnant WT female mice were injected with inflammasome inhibitors (VX-765 or
788 MCC950 to inhibit CASP1 or NLRP3, respectively) or control (Vehicle) at E12.5, E13.5,
789 and E14.5. Behaviors of the male offspring of injected mice were tested at 8-weeks old.
790 **B**. General activity of the male offspring of control- (vehicle; black circles, N=11, from 3
791 litters), VX-765- (blue diamonds, N=10, from 3 litters), and MCC950-injected mothers
792 (pink triangles, N=8, from 3 litters) was determined by open field assay and is shown as
793 the total distance moved (centimeters, cm). *p*=0.0412, DF=28, F=3.614. Tukey's
794 multiple comparison test: Veh vs VX-765 *p*-0.0963, Veh vs MCC950 *p*=0.0591, VX-765
795 vs MCC950 *p*=0.9250. Dots indicate individual animals and error bars indicate S.E.M.
796 **C**. Anxiety levels in the indicated offspring were determined by elevated plus maze
797 assay and are shown as time spent in open arms (sec). *p*=0.0325, DF=28, F=3.92.
798 Tukey's multiple comparison test: Veh vs VX-765 *p*=0.1736, Veh vs MCC950 *p*=0.0307,
799 VX-765 vs MCC950 *p*=0.6151. Data is shown as individual animals and error bars
800 indicate S.E.M. Asterisk (*) indicates *p*<0.05 and n.s. indicates not significant. **D.**
801 Working model is shown. Activation of the NLRP3-CASP1-GSDMD/IL-1β cascade in
802 fetal microglia is required for normal brain development. Genetic or pharmacological
803 disruption of this pathway results in aberrant behaviors.

804 **Movies legend**
805
806 **Movies 1 and 2.**

807 Representative light sheet fluorescence microscopy imaging of male E14.5 WT (Movie
808 1) and *Casp1*$^{-/-}$ fetal brains (Movie 2). Embryos had one copy of *Cx3cr1*-GFP and were
809 injected with PI 10-30 minutes before tissue harvest and visualization. Movies show
810 sequential z-planes of a typical acquisition followed by 3D maximum intensity projection.
811 Purple: PI. Green: *Cx3cr1*-GFP, White: Merged.

812

813 **Table legend**

814 **Table 1. Behavior assays.**

815 The information on primary antibodies used in this study is shown.

816

817 **Table 2. Information on primary antibodies.**

818 The behavior assays used in this study are shown.

819

820 **Table 3. Information for Student's *t*-tests.** For the Student's *t*-tests used in our
821 analyses, the *t*-values, degrees of freedom (df), and *p*-values are summarized.

822

823 **Table 4. Information for one-way ANOVA.** For our one-way ANOVA analyses, the
824 sum-of-squares (SS), degrees of freedom (DF), the mean squares (MS), F ratios, and
825 *p*-values used to assess the variation between columns, within columns, and total are
826 summarized.

827

828 **Extended Figure Legends**
829
830 **Figure 1-1. Inflammasome cascade and attention behavior of *Casp1*$^{-/-}$ mice. A.**
831 Diagram of the inflammasome cascade. NLRP3, an inflammasome protein, is activated
832 and provides a platform to cleave pro-CASP1 to generate CASP1. CASP1 cleaves pro-
833 gasdermin D to gasdermin D (GSDMD), which assembles and generates pores in the
834 plasma membrane and induces lytic cell death. CASP1 also cleaves pro-IL-1β to
835 generate mature IL-1β cytokine. **B, G, and I.** Elevated plus maze assay results from the
836 indicated male mice to support Figure 1B, D, and F are shown as the time spent in open
837 arms compared to the total time spent on the apparatus (%). **C, H, and J.** Elevated plus
838 maze assay results from the indicated male mice to support Figure 1B, D, and F are
839 shown as the number of entries into open arms compared to the total number of entries
840 (%). **D.** Attention behavior of male WT (N=7, black circles, from 3 litters) and *Casp1*$^{-/-}$
841 (N=10, red triangles, from 4 litters) mice was determined by the five-choice serial
842 reaction time task and is shown as the accuracy of their responses (%). **E.** General
843 activity of female WT (black circles, N=4, from 2 litters) and *Casp1*$^{-/-}$ (red squares, N=3,
844 from 2 litters) mice was determined by open field assay and is shown as total distance
845 moved (centimeters, cm). **F.** Anxiety levels of female WT (black circles, N=5) and
846 *Casp1*$^{-/-}$ (red squares, N=4) mice were determined using the elevated plus maze assay
847 and are shown as the time spent in open arms (sec). Dots indicate individual animals
848 and error bars show S.E.M. (B) p=0.0029, df=21, t=3.371. (C) p=0.0002, df=21, t=4.425.
849 (D) p=0.028, df=15, t=2.432. (E) p=0.5129, df=5, t=0.704. (F) p=0.9829, df=7, t=0.022.
850 (G) p=0.0050, DF=33, F=6.304. Tukey's multiple comparison test: WT vs *Il-1r*$^{-/-}$
851 p=0.1809, WT vs *Gsdmd*$^{-/-}$ p=0.0036, *Il-1r*$^{-/-}$ vs *Gsdmd*$^{-/-}$ p=0.2729. (H) p=0.1518, DF=33,

F=2.005. Tukey's multiple comparison test: WT vs *Il-1r*$^{-/-}$ p=0.2964, WT vs *Gsdmd*$^{-/-}$ p=0.1717, *Il-1r*$^{-/-}$ vs *Gsdmd*$^{-/-}$ p=0.9610. (I) p=0.0130, df=17, t=2.776. (J) p=0.0035, df=17, t=3.392. Asterisk (*) indicates p<0.05, (**) indicates p<0.01, and n.s. indicates not significant.

Figure 2-1. *Casp1* is expressed in microglia from fetal brains and adult *Casp1*$^{-/-}$; *iCasp1*; *Cx3cr1*-Cre mice. A-D. mRNA expressions of *Casp1* (**A**), *Nlrp3* (**B**), *Cd200* (**C**), and *Celf4* (**D**) in *Cx3cr1*-GFP^{+} and *Cx3cr1*-GFP^{-} cells from male fetal brain at E14.5, as determined by RT-qPCR. (A) p<0.0001, df=2, t=688.100. (B) p<0.0001, df=2, t=1319.000. (C) p<0.0001, df=2, t=598.900. (D) p<0.0001, df=2, t=220.900. Data is shown as the average of duplicates and error bars indicate S.E.M. **E.** Microglial cells were isolated from the brains of adult male WT (black circles), Control (blue rectangles), and Experimental (red rectangles) mice and the mRNA expressions of *Casp1* were determined by RT-qPCR. **F.** Elevated plus maze assay results supporting Figure 2C are shown as the time spent in open arms compared to the total time spent on the apparatus (%). **G.** Elevated plus maze assay results supporting Figure 2C are shown as the number of entries into open arms compared to the total number of entries (%). (E) p=0.0015, DF=10, F=16.19. Tukey's multiple comparison test: WT vs Control p=0.2260, WT vs Experimental p=0.0230, Control vs Experimental p=0.0013. (F) p<0.0001, DF=28, F=15.92. Tukey's multiple comparison test: WT vs Control p<0.0001, WT vs Experimental p=0.0759, Control vs Experimental p=0.0024. (G) p=0.0330, DF=28, F=3.902. Tukey's multiple comparison test: WT vs Control p=0.0743, WT vs Experimental p=0.0340, Control vs Experimental p=0.9469. Data indicates individual

875 mice and averages are shown. Error bars indicate S.E.M. (**) indicates $p<0.01$ and
876 (****) indicates $p<0.0001$.
877
878 **Figure 3-1. Quantification and qualification of clusters in WT and *Casp1* re-**
879 **expression mice. A.** Numbers of WT mice (male, N=6) that exhibited clusters in the
880 LGE and iTh at E12.5 are shown. n.s. indicates not significant. **B.** Cell numbers in the
881 clusters from the LGE and iTh at E14.5 are shown. **C.** A representative brightfield image
882 of the cluster including swollen microglial cells. Scale bar indicates 100 μm. **D.**
883 Diameters of GFP^+ and GFP^+PI^+ cells in the clusters are shown. $p=0.0005$, df=30,
884 $t=3.935$. Diameters of individual cells and the averages are shown. Error bars indicate
885 S.E.M. (***) indicates $p<0.001$. **E.** *Casp1*$^{-/-}$; *iCasp1*; *Cx3cr1*-Cre mice express GFP upon
886 Cre-mediated recombination. Mice were injected with PI as shown in Figure 3A.
887 Representative brightfield (top left), *Cx3cr1*-GFP staining signal (top right), PI signal
888 (bottom left), and merged (bottom right) images are shown. Scale bar in the bright field
889 image indicates 230 μm and the others indicate 130 μm.
890
891 **Figure 4-1. Brain volume does not change in *Casp1*$^{-/-}$ mice.** Volumes of the
892 cerebrum, thalamus, and striatum of adult male WT (black circles) and *Casp1*$^{-/-}$ (red
893 triangles) mouse brains were determined by Nissl staining and stereology. Cerebrum
894 $p=0.8580$, df=4, $t=0.191$. Thalamus $p=0.5247$, df=4, $t=0.691$. Striatum $p=0.9372$, df=4,
895 $t=0.084$. Data is shown as volumes (μm^3) of regions from individual mice and their
896 averages. Error bars indicate S.E.M. and n.s. indicates not significant.
897

Figure 5-1. Evaluation of inhibitor-exposed offspring in the elevated plus maze and our working model of the role of lytic microglial death in NPC development. A. Elevated plus maze assay results supporting Figure 5C are shown as the time spent in open arms compared to the total time spent on the apparatus (%). **B.** Elevated plus maze assay results supporting Figure 5C are shown as the number of entries into open arms compared to the total number of entries (%). (A) p=0.0325, DF=28, F=3.921. Tukey's multiple comparison test: Veh vs VX-765 p=0.1736, Veh vs MCC950, p=0.0307, VX-765 vs MCC950 p=0.6151. (B) p=0.1981, DF=28, F=1.724. Tukey's multiple comparison test: Veh vs VX-765 p=0.4081, Veh vs MCC950 p=0.2001, VX-765 vs MCC950 p=0.8550. Asterisk (*) indicates p<0.05 and n.s. indicates not significant **C.** A cartoon describing our working model of the fetal brain iTh at E14.5. Damage-associated molecular patterns (DAMPs), such as ATP, are released from dead or dying neural cells to activate microglial NLRP3 and initiate the NLRP3-CASP1-GSDMD/IL-1β cascade depicted in Figure 5D. As a result, sterile inflammation (perhaps mediated in part by IL-1β) influences the development of neural precursor cells (NPCs). We propose that proinflammatory cytokines are required to promote the death of TRN precursor cells in the iTh, which is why we observe increased numbers of neurons in the TRN region of adult *Casp1*$^{-/-}$ brains.

Figure 1

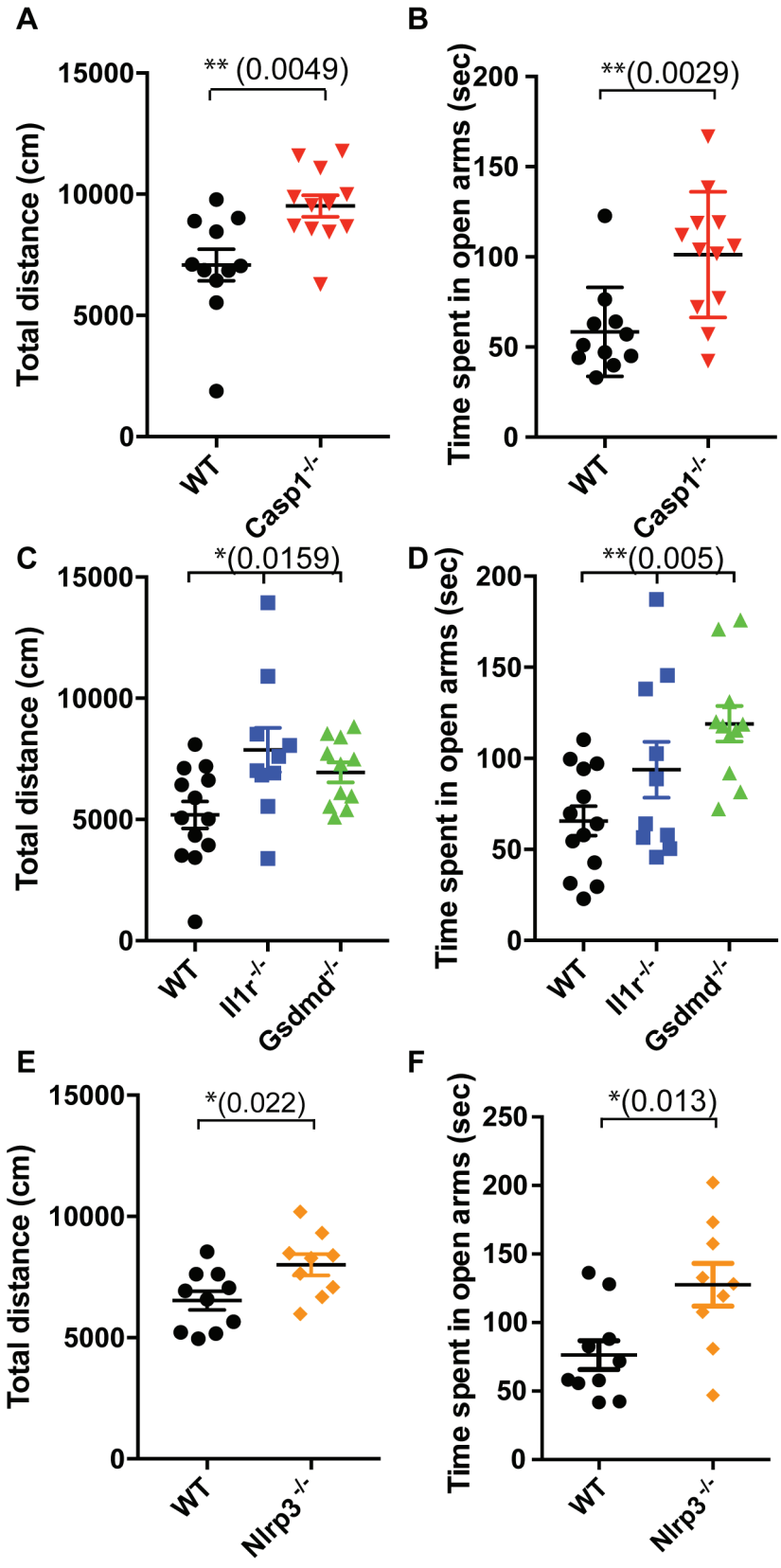

Figure 2

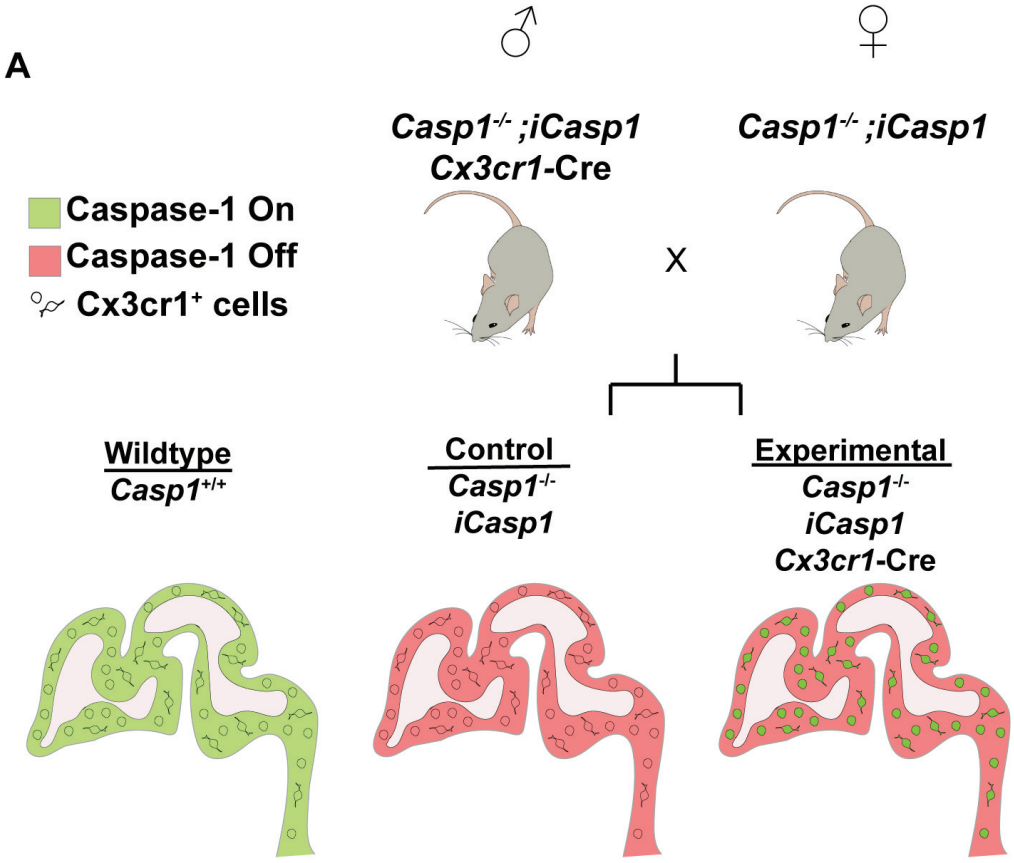

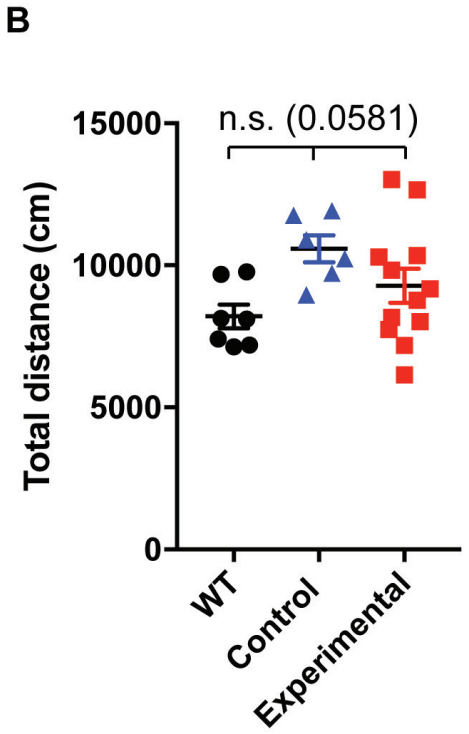

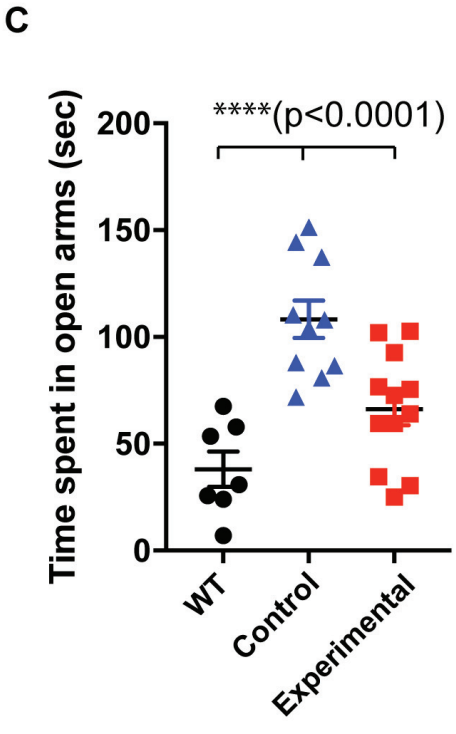

Figure 3

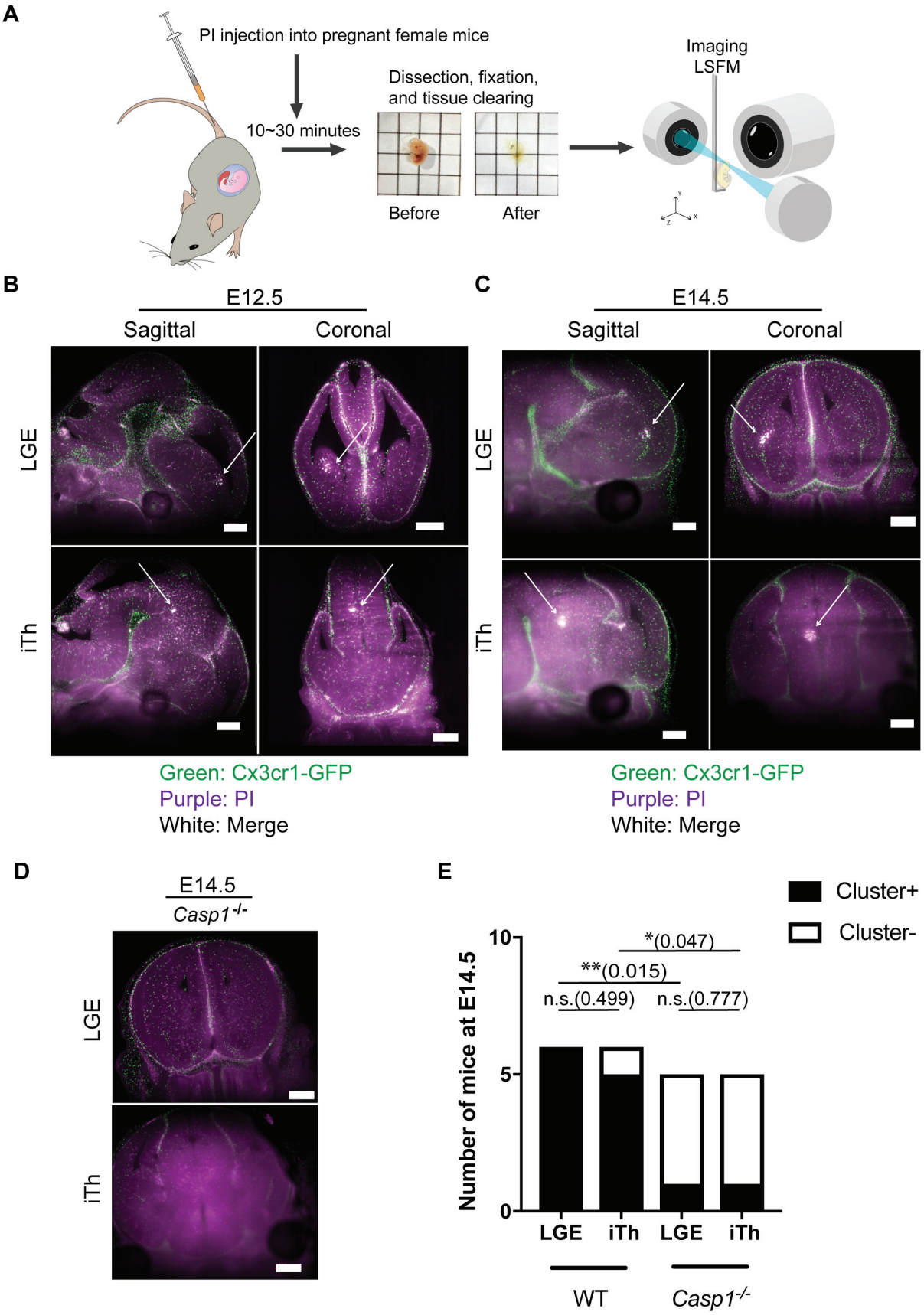

Figure 4

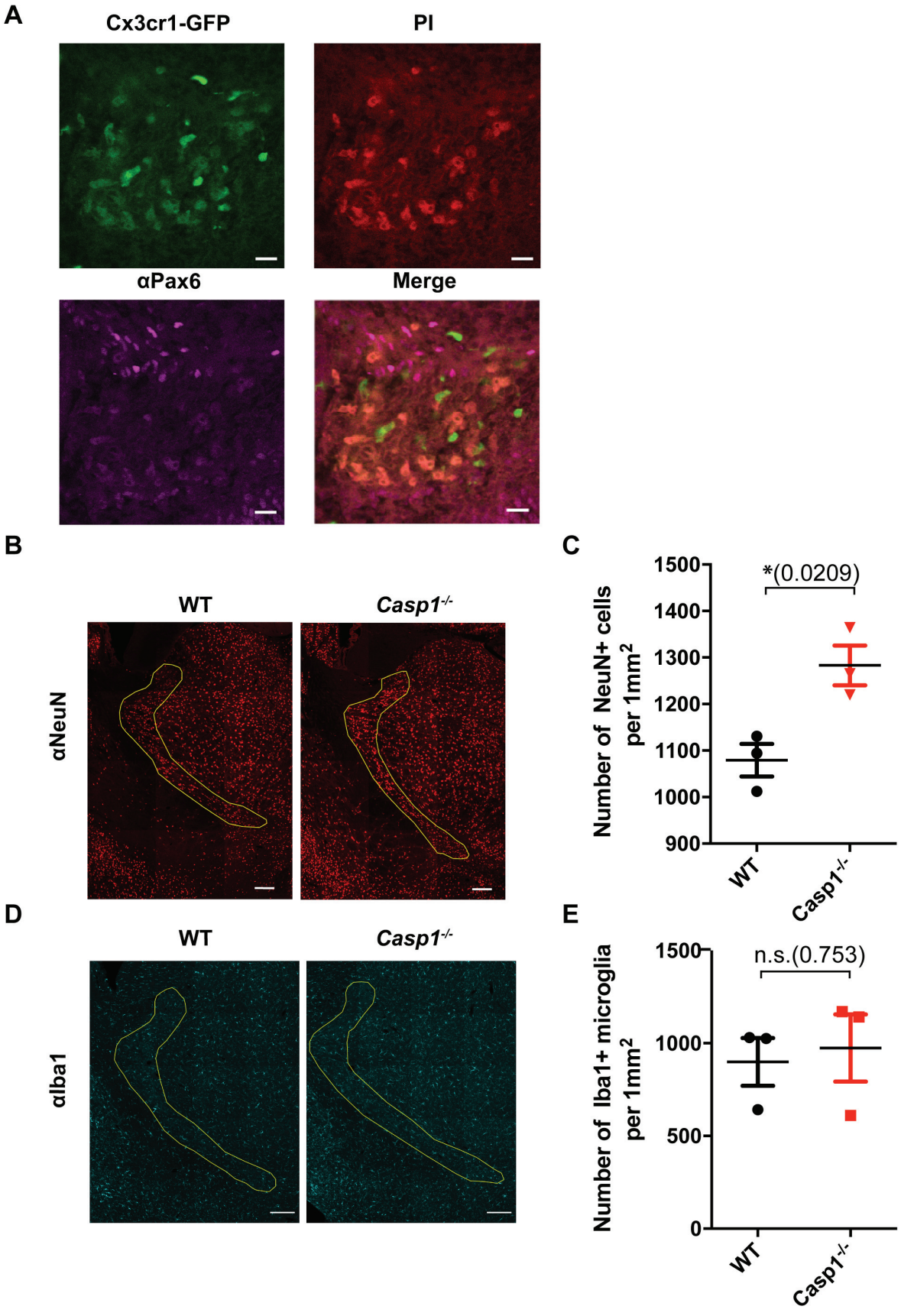

Figure 5

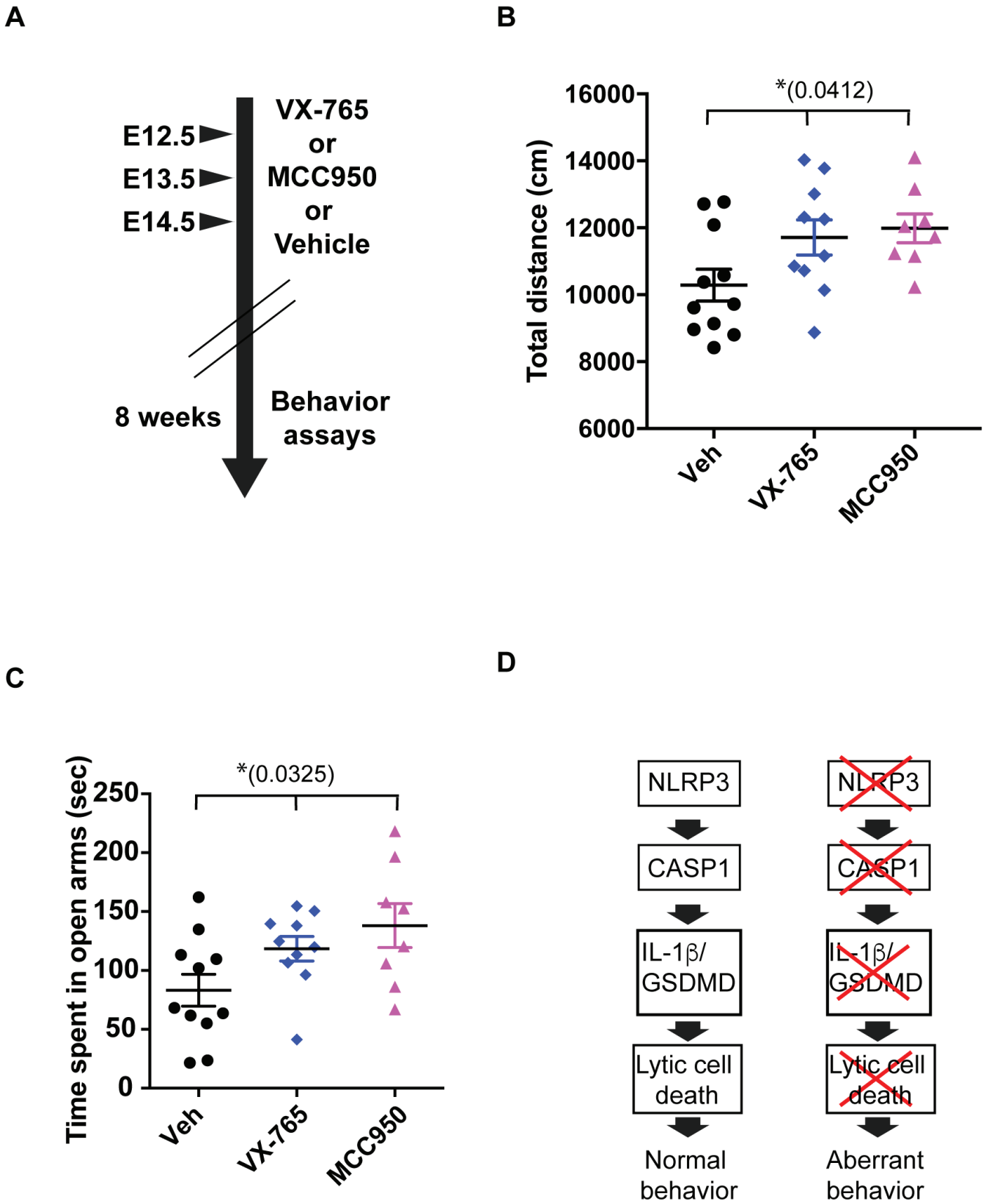

Table 1.

Behavior	Assay
Hyperactivity	Open field assay (Total distance they moved)
Anxiety	Elevated plus maze assay
Attention	Five-choice serial reaction time task assay

Table 2.

Name	Vendor	Catalog No.	Dilution
NeuN	Millipore Sigma	ABN78	1:300
Parvalbumin	Millipore Sigma	P3088	1:1000
Iba1	Thermo Fisher	PA5-18039	1:250
Pax6	Eurogentec	PRB-278P-100	1:100

Table 3.

Figure	*t*-value	df	*p*-value
1A	3.142	21	0.0049
1B	3.371	21	0.0029
1E	2.520	17	0.0220
1F	2.776	17	0.0130
4C	3.694	4	0.0209
4E	0.336	4	0.7533
1-1B	3.371	21	0.0029
1-1C	4.425	21	0.0002
1-1D	2.432	15	0.0280
1-1E	0.704	5	0.5129
1-1F	0.022	7	0.9829
1-1I	2.776	17	0.0130
1-1J	3.392	17	0.0035
2-1A	688.100	2	<0.0001
2-1B	1319.000	2	<0.0001
2-1C	598.900	2	<0.0001
2-1D	220.900	2	<0.0001
3-1D	3.935	30	0.0005
4-1 Cerebrum	0.191	4	0.8580
4-1 Thalamus	0.691	4	0.5274
4-1 Striatum	0.084	4	0.9372

Table 4.

1C	**SS**	**DF**	**MS**	**F (DFn, DFd)P**	
between columns	43308629	2	21654315	F (2, 31) = 4.748	*p*=0.0159
within columns	141389895	31	4560964		
total	184698524	33			
1D					
between columns	17029	2	8514	F (2, 31) = 6.306	*p*=0.0050
within columns	41856	31	1350		
total	58885	33			
2B					
between columns	18214401	2	9107200	F (2, 22) = 3.247	*p*=0.0581
within columns	61708704	22	2804941		
total	79923105	24			
2C					
between columns	21480	2	10740	F (2, 26) = 15.97	*p*<0.0001
within columns	17489	26	672.7		
total	38969	28			
5B					
between columns	2577676	2	1288838	F (2, 26) = 3.614	*p*=0.0412
within columns	9272962	26	356652		
total	11850639	28			
5C					
between columns	14905	2	7453	F (2, 26) = 3.92	*p*=0.0325
within columns	49424	26	1901		
total	64329	28			
1-1G					
between columns	473	2	236.5	F (2, 31) = 6.304	*p*=0.0050
within columns	1163	31	37.51		
total	1636	33			
1-1H					

between columns	136.1	2	68.07	F (2, 31) = 2.005	*p*=0.1518
within columns	1053	31	33.96		
total	1189	33			
2-1E					
between columns	11.75	2	5.876	F (2, 8) = 16.19	*p*=0.0015
within columns	2.904	8	0.363		
total	14.66	10			
2-1F					
between columns	597.6	2	298.8	F (2, 26) = 15.92	*p*<0.0001
within columns	488	26	18.77		
total	1086	28			
2-1G					
between columns	230.5	2	115.3	F (2, 26) = 3.902	*p*=0.0330
within columns	768	26	29.54		
total	998.5	28			
5-1B					
between columns	414	2	207	F (2, 26) = 3.921	*p*=0.0325
within columns	1373	26	52.8		
total	1787	28			
5-1C					
between columns	78.67	2	39.34	F (2, 26) = 1.724	*p*=0.1981
within columns	593.2	26	22.82		
total	671.9	28			